communications biology

Article

https://doi.org/10.1038/s42003-024-07429-2

FOXG1 promotes osteogenesis of bone marrow-derived mesenchymal stem cells by activating autophagy through regulating USP14

Check for updates

Yiqi Zhang[1], Long Zhou[1], Qin Fu[1] & Ziyun Liu[2]

The osteogenic differentiation of bone marrow-derived mesenchymal stem cells (BMSCs) is key for bone formation, and its imbalance leads to osteoporosis. Forkhead Box Protein G1 (FOXG1) is associated with osteogenesis, however, the effect of FOXG1 on osteogenesis of BMSCs and ovariectomy (OVX)-induced bone loss is unknown. In our study, FOXG1 expression in BMSCs increases after osteogenic induction. FOXG1 overexpression significantly increases osteoblast marker expression ALP activity, and calcium deposition, while the opposite results are observed in FOXG1 knockdown BMSCs, suggesting that FOXG1 promotes osteogenic differentiation. Additionally, autophagy promotes the differentiation process in BMSCs. We find that FOXG1 induces autophagy, and osteogenic differentiation is blocked via inhibiting FOXG1-caused autophagy, indicating that FOXG1 accelerates osteogenic differentiation via inducing autophagy. Eight-week-old female C57BL/6J mice are used in OVX models, FOXG1 overexpression decreases bone loss by increasing bone formation. Moreover, FOXG1 overexpression suppresses osteoclast differentiation. Mechanically, FOXG1 transcriptionally represses ubiquitin-specific protease14 (USP14) via binding to the USP14 promoter. USP14 overexpression prevents the promoting effect of FOXG1 on osteogenic differentiation in BMSCs. Therefore, our findings suggest that FOXG1 promotes BMSC osteogenic differentiation and inhibits osteoclast differentiation, eventually blocking OVX-induced bone loss, which may provide a promising approach for osteoporosis treatment.

Osteoporosis is a common bone metabolic disease in the elderly population and postmenopausal women. Its main characteristics are impaired bone architecture and low mineral density, which increases the risk of fractures[1]. Bone marrow-derived mesenchymal stem cells (BMSCs) are the precursor cells to osteoblast and adipocyte[2]. In patients with osteoporosis, the osteogenic differentiation ability of BMSCs is weakened[3]. Thus, restoring the osteogenic differentiation ability of BMSCs is an important means to treat osteoporosis and has vital significance in improving the prognosis of osteoporosis patients.

Forkhead Box Protein G1 (FOXG1), one of the members of the Forkhead family, often acts as a transcriptional repressor[4]. FOXG1 plays a crucial role in multiple physiological and pathological processes, such as presbycusis[5], neurodevelopmental disorders[6], and cancers[7]. However, the effect of FOXG1 on osteoporosis has not been clarified yet. It has been reported that FOXG1 is involved in the osteoblast differentiation process[8], and it is highly expressed in BMSCs of elderly patients with osteoporosis via bioinformatics analysis[9], suggesting that FOXG1 may regulate the procession of BMSCs in osteoporosis. Moreover, autophagy significantly promotes the differentiation of BMSCs and improves bone loss in osteoporosis[10]. Inhibition of FOXG1 reduces the activity of autophagy, resulting in the accumulation of reactive oxygen species (ROS)[5,11]. Thus, we speculated that FOXG1 may affect osteoporosis progression by regulating the autophagy of BMSCs.

Ubiquitin-specific protease14 (USP14) as a deubiquitinating enzyme (DUB), negatively regulates the activity of proteasomes through trimming the ubiquitin chain on the proteasome-bound substrates[12,13]. Recent findings show that USP14 influences other cellular processes, including autophagy[14]. USP14 regulates autophagy via inhibiting K63 ubiquitin of Beclin 1[15]. Besides, USP14 suppression induces endoplasmic reticulum stress-mediated autophagy by activating c-Jun N-terminal kinase 1 (JNK1)[16].

[1]Department of Orthopedics, Shengjing Hospital of China Medical University, Shenyang, Liaoning, China. [2]Department of Pediatrics, Shengjing Hospital of China Medical University, Shenyang, Liaoning, China. e-mail: liuziyuncmu@sj-hospital.org

Notably, research has shown that USP14 inhibition protects osteoblastic cells against dexamethasone (DEX)-induced apoptosis[17], indicating that USP14 may be a potential target for osteoporosis treatment. In this study, we predicted FOXG1 had binding sites on the USP14 promoter through bioinformatic analysis. Therefore, we guessed that the FOXG1/USP14 axis is involved in osteoporosis progression.

In this study, we examined the expression level of FOXG1 in bone and BMSCs from ovariectomized (OVX) mice, and its function in mice-derived BMSCs. Finally, we confirmed the regulatory mechanism of FOXG1.

Results

FOXG1 promotes osteogenic differentiation of mice-derived BMSCs

To evaluate the function of FOXG1 in osteogenesis by BMSCs, BMSCs were isolated and identified by flow cytometry (Supplementary Fig. 1). BMSCs were cultured with osteogenic medium (OM) for 0, 3, 7, and 14 days, and the results exhibited that FOXG1 expression was increased along the time of differentiation (Fig. 1A). Then, FOXG1 was overexpressed or knocked down in BMSCs by infecting with FOXG1 overexpression lentivirus or shFOXG1 lentivirus, respectively. The results of RT-qPCR and western blot confirmed the successful establishment of FOXG1 overexpression (Fig. 1B) and knockdown BMSCs (Fig. 1C). The osteogenic differentiation of BMSCs was assessed by ALP activity assay. ALP activity was increased in BMSCs cultured in OM, compared to those cultured in normal medium (NM). It was noted that FOXG1 overexpression further increased ALP activity in BMSCs cultured in OM, while FOXG1 knockdown decreased ALP activity in BMSCs cultured in OM (Fig. 1D). Besides, the expression of osteoblast markers Col1A1, OCN, OPN, and Runx2 was upregulated during osteogenesis. FOXG1 overexpression induced even higher expression of these markers compared to the OM group, whereas the opposite results were observed when FOXG1 was knocked down (Fig. 1E). Meanwhile, Alizarin red staining also confirmed that FOXG1 overexpression enhanced calcium deposition but FOXG1 knockdown reduced calcium deposition during osteogenic differentiation (Fig. 1F–G). There results indicated that FOXG1 promoted osteogenic differentiation in BMSCs.

FOXG1 promotes autophagy in BMSCs

Autophagy promotes the differentiation process in BMSCs and also affects the survival of osteoblasts. We found that FOXG1 overexpression promotes osteoblast viability, whereas its knockdown inhibited osteoblast viability (Supplementary Fig. 2A). Additionally, TEM results showed that increased autophagosomes were observed upon OM treatment. Autophagosomes were identified based on double-membrane structures containing internal contents. We found that more autophagosomes were generated in FOXG1 overexpression BMSCs, while FOXG1 knockdown reduced the ability of autophagosome form (Fig. 2A). Osteogenic differentiation induced the augmentation of autophagy, which was confirmed by the upregulated mRNA expression of Beclin1 and LC3. Their expression was further upregulated when FOXG1 was overexpressed. In contrast, FOXG1 knockdown downregulated their expression (Fig. 2B). Similarly, the results of western blot exhibited that FOXG1 overexpression upregulated the expression of Beclin1 and LC3-II/LC3-I ratio, as well as the attenuated p62 expression, but the opposite results were obtained by knocking down (Fig. 2C). Furthermore, we implemented IF stain to investigate the influence of FOXG1 on puncta formation of LC3 in BMSCs, the results revealed that LC3 puncta significantly increased upon FOXG1 overexpression while FOXG1 knockdown decreased puncta formation (Fig. 2D). These findings implied that FOXG1 promoted autophagy in BMSCs.

FOXG1 induces osteogenic differentiation by regulating autophagy in BMSCs

To confirm whether FOXG1 influences osteogenic differentiation by autophagy, we added the autophagy inhibitor 3-MA or the autophagy activator Rapamycin (Rapa) to FOXG1 overexpression or knockdown BMSCs, respectively. The results showed that the increased ALP activity induced by FOXG1 overexpression was inhibited by 3-MA, whereas ALP activity blocked by FOXG1 knockdown was promoted by Rapa (Fig. 3A). Besides, FOXG1 overexpression promoted the expression of Col1A1, OCN, OPN, and Runx2, but this effect was suppressed in cultures treated with 3-MA. FOXG1 knockdown led to the downregulated expression of these markers, while these expression changes were reversed by Rapa (Fig. 3B). Alizarin red staining displayed that FOXG1 overexpression induced more calcium deposition than the OM control, however, a supplement of 3-MA, significantly repressed calcium deposition. Moreover, reduced calcium deposition in FOXG1 knockdown BMSCs and the presence of Rapa increased calcium deposition (Fig. 3C). We used another autophagy inhibitor chloroquine (CQ) to further verify the involvement of functional autophagy in FOXG1-mediated regulation of osteogenesis. We found that increased ALP activity induced by FOXG1 overexpression was inhibited by CQ (Supplementary Fig. 2B). Alizarin red staining revealed that FOXG1 overexpression induced more calcium deposition, but this trend was suppressed after CQ treatment (Supplementary Fig. 2C). These results indicated that FOXG1 induced osteogenic differentiation by regulating autophagy.

USP14 inhibits osteogenic differentiation of mice-derived BMSCs

USP14 suppresses autophagy and its inhibition exerts a protective effect on osteoblast damage[17,18]. Thus, we speculated that USP14 may be involved in the osteogenic differentiation of BMSCs. BMSCs were cultured OM for 0, 3, 7, and 14 days, and the results of western blot exhibited that USP14 expression was decreased along the time of differentiation (Fig. 4A). ALP and Alizarin red staining confirmed that USP14 overexpression decreased ALP activity and mineralization after osteogenic induction (Fig. 4B, C). On the contrary, USP14 knockdown in BMSCs showed contrary results (Fig. 4D, E). These findings suggested that USP14 inhibited osteogenic differentiation.

FOXG1 inhibits the transcription of USP14

Through bioinformatics analysis, we predicted that FOXG1 may regulate the transcription of USP14. To investigate the relationship between FOXG1 and USP14, the expression of USP14 was detected in FOXG1 overexpression or knockdown BMSCs. The results revealed that FOXG1 overexpression downregulated USP14 expression (Fig. 5A), while FOXG1 knockdown upregulated USP14 expression (Fig. 5B). We predicted the possible binding sites of FOXG1 on the USP14 promoter (Fig. 5C), and verified by dual-luciferase reported assays. We tried to identify the binding sites of FOXG1 by truncating regions within the USP14 promoter. The results revealed that the promoter activity was significantly changed by all three FOXG1 binding sites (Fig. 5D). The subsequent ChIP-qPCR assays further confirmed the direct interaction between FOXG1 and the USP14 promoter (Fig. 5E). These results suggested that FOXG1 inhibited the transcription of USP14.

FOXG1 promotes autophagy and osteogenic differentiation by regulating USP14 in BMSCs

To demonstrate whether FOXG1 affects BMSCs by regulating USP14, USP14 overexpression BMSCs were constructed and the western blot was performed to confirm successful overexpression of USP14 (Fig. 6A). Next, BMSCs were co-infected with USP14 overexpression lentivirus and FOXG1 overexpression lentivirus. We found that FOXG1 overexpression enhanced ALP activity, but ALP activity was blocked by USP14 overexpression (Fig. 6B). The expression of Col1A1, OCN, OPN, and Runx2 was upregulated by FOXG1 overexpression, nevertheless, it was also suppressed with USP14 overexpression (Fig. 6C). In addition, calcium deposition was enhanced upon FOXG1 overexpression, consistently, USP14 overexpression decreased calcium deposition (Fig. 6D). As for autophagy, FOXG1 overexpression elicited significant augmentation of Beclin1 expression and LC3-II/LC3-I ratio, and weakened p62 expression, although this effect was reversed by USP14 overexpression (Fig. 6E). Our data elucidated that FOXG1 promotes autophagy and osteogenic differentiation by inhitiing USP14.

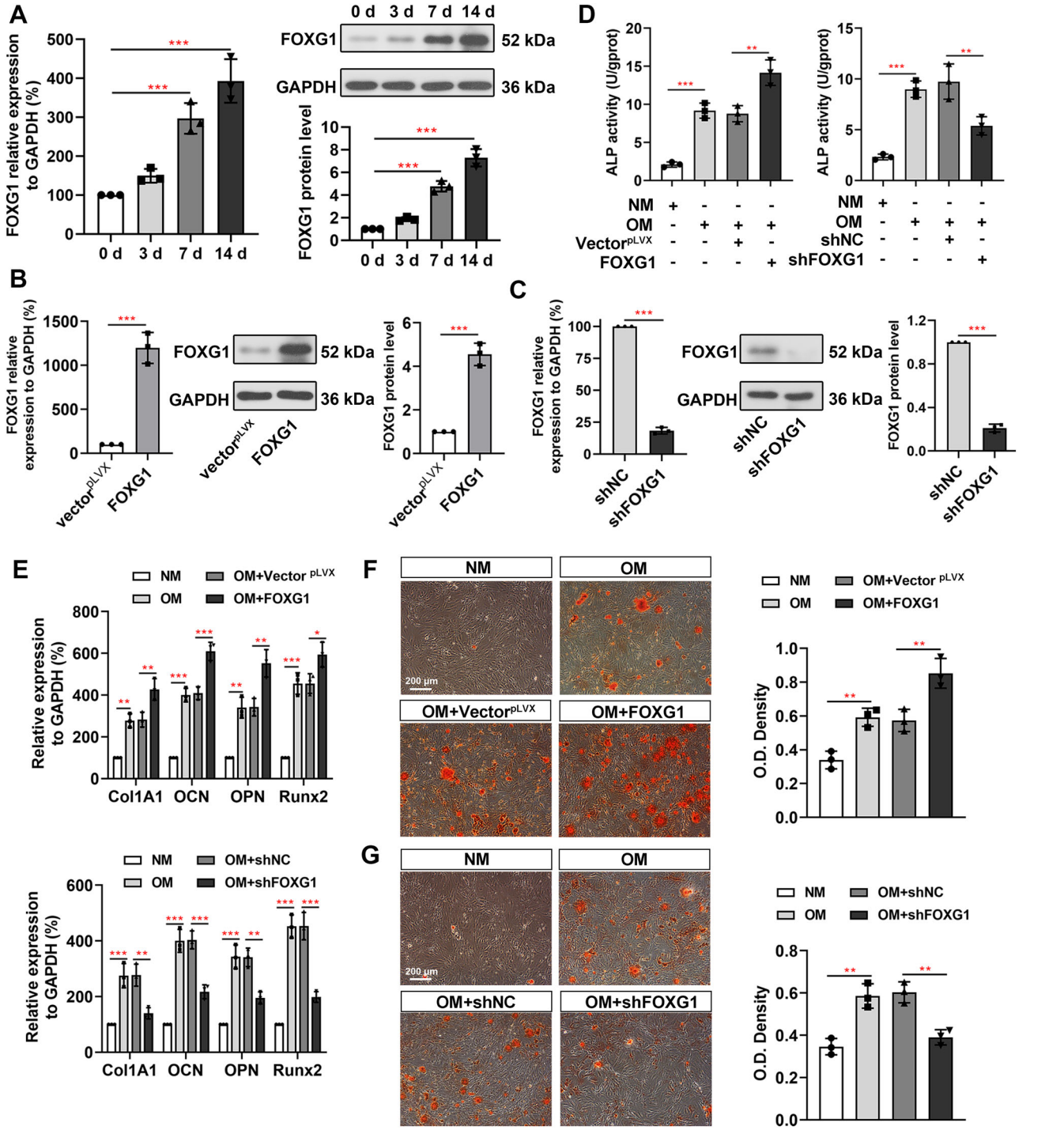

Fig. 1 | FOXG1 promotes osteogenic differentiation of mice-derived BMSCs. **A** BMSCs were incubated in osteogenic medium (OM) for 0, 3, 7, or 14 days, then, the mRNA and protein expression levels of FOXG1 were detected by RT-qPCR and western blot. **B**, **C** BMSCs were infected with FOXG1 overexpression lentivirus (FOXG1) or shFOXG1 lentivirus (FOXG1), 48 h after infection, and the mRNA and protein expression levels of FOXG1 were detected by RT-qPCR and western blot. **D** After lentivirus infection, BMSCs were cultured in normal medium (NM) or OM, then, ALP activity was detected using an ALP activity detection kit. **E** The mRNA expression levels of Col1A1, OCN, OPN, and Runx2 were detected by RT-qPCR. **F**, **G** The calcium deposition was determined by Alizarin red staining. Scale bar, 200 μm. Data represented mean ± SD ($n = 3$ biological replicates). $^{*}P < 0.05$; $^{**}P < 0.01$; $^{***}P < 0.001$.

FOXG1 expression is upregulated in OVX mice-derived BMSCs

Through bioinformatics analysis, we found that FOXG1 was upregulated in BMSCs of osteoporosis patients (Supplementary Fig. 3A). Therefore, to investigate the role of FOXG1 in osteoporosis, the OVX mouse model was established (Supplementary Fig. 3B). Micro-CT demonstrated that extensive bone loss was observed in OVX mice (Supplementary Fig. 3C). Quantitative analysis of bone parameters also verified decreased bone mineral density (BMD), bone volume/total volume (BV/TV), trabecular thickness (Tb. Th) and trabecular bone number, and increased trabecular space (Tb. Sp) (Supplementary Fig. 3D) in OVX mice relative to sham mice. Additionally, increased bone loss was confirmed in OVX mice compared with the sham group by H&E staining (Supplementary Fig. 3E). Furthermore, BMSCs were isolated from the femurs of mice in the Sham or OVX group, and flow cytometry was used to characterize BMSCs. Results showed

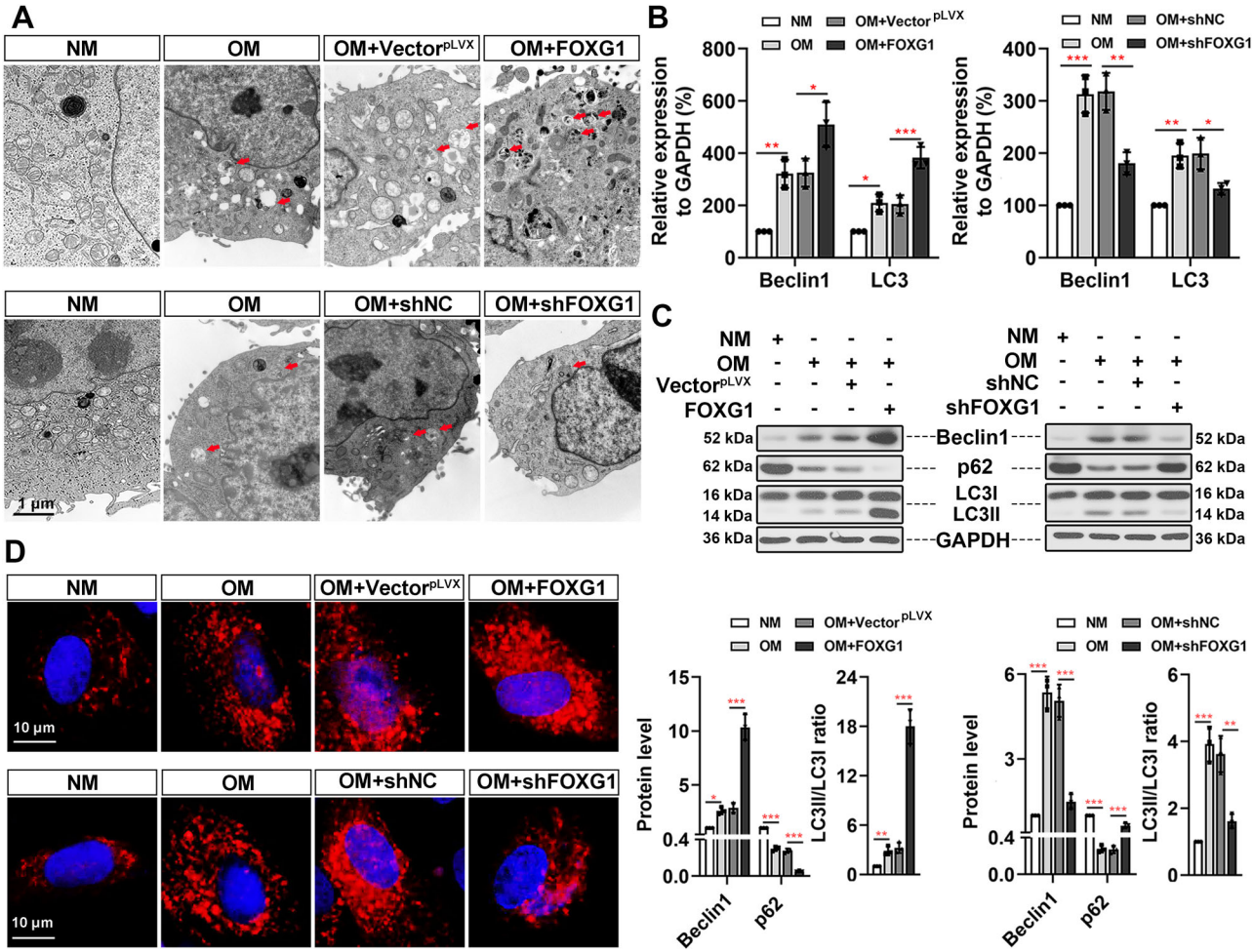

Fig. 2 | FOXG1 promotes autophagy in BMSCs. A The autophagosomes were observed by transmission electron microscopy (TEM). The red arrow indicates a double membrane autophagosome. Scale bar, 1 μm. **B** The mRNA expression levels of Beclin1 and LC3 were detected by RT-qPCR. **C** The protein expression levels of Beclin1, p62, and LC3I/II were detected by western blot. **D** The LC3 puncta was detected by immunofluorescence staining (IF). Scale bar, 10 μm. Data represented mean ± SD ($n = 3$ biological replicates). $^{*}P < 0.05$; $^{**}P < 0.01$; $^{***}P < 0.001$.

that > 90% of cells were $CD29^{+}$ and $CD90^{+}$, whereas $CD34^{+}$ and $CD45^{+}$ were very low (<4%) (Supplementary Fig. 4). We also assessed the mRNA and protein levels of FOXG1 and found that OVX mice-derived BMSCs showed a significant increase in FOXG1 expression compared to sham mice (Fig. 7A, B). These findings suggested that FOXG1 was highly expressed in OVX mice-derived BMSCs.

FOXG1 promotes osteogenic differentiation in OVX-induced osteoporosis mice

To investigate the effect of FOXG1 in vivo, FOXG1 overexpression mice were established (Fig. 7C), and the results of the western blot revealed the successful infection of FOXG1 in the femoral bone (Supplementary Fig. 5A). Micro-CT demonstrated that FOXG1 overexpression prevented the extensive bone loss caused by the OVX procedure in mice femurs (Fig. 7D), shown by the increased BMD, BV/TV, Tb. Th, and Tb. N, and reduced Tb.Sp (Fig. 7E). H&E staining revealed that FOXG1 overexpression decreased the extent of bone loss induced by OVX (Fig. 7F). Then, immunohistochemical staining of FOXG1 and OB marker Osteocalcin was performed. The results showed that FOXG1 expression was upregulated, and Osteocalcin expression was downregulated in OVX mice, we did not observe obvious co-localization. Whereas in OVX + AAV-FOXG1, the co-localization of FOXG1 and Osteocalcin increased (Supplementary Fig. 5B). We speculate that FOXG1 upregulation may be a protective response in the occurrence of osteoporosis, but its endogenous upregulation is not sufficient to prevent decreased bone formation under pathophysiological conditions. After upregulating FOXG1 expression using an AAV, bone formation was promoted. We also assessed the expression of Col1A1, OCN, OPN, and Runx2. Their expressions were suppressed after the OVX procedure, but FOXG1 overexpression in OVX mice dramatically reversed this effect (Fig. 7G). BMSCs were also harvested from the femur tissues of mice and the surface markers of BMSCs were determined by flow cytometry (Supplementary Fig. 5C). The mRNA and protein expression of FOXG1 was upregulated after the OVX procedure, which was further enhanced when FOXG1 was overexpressed (Fig. 8A, B). Additionally, the expression of USP14 level increased in OVX mice but decreased in OVX mice with FOXG1 overexpression (Fig. 8C). OVX procedure led to decreased ALP activity than that in BMSCs derived from sham mice, whereas FOXG1 overexpression enhanced ALP activity (Fig. 8D). Beclin1 expression and LC3-II/LC3-I ratio were decreased, and p62 expression was increased in BMSCs derived from OVX mice, although this effect was reversed by FOXG1 overexpression (Fig. 8E). Furthermore, Alizarin red staining confirmed that calcium deposition in OVX mice-derived BMSCs was reduced, nevertheless, it was enhanced with FOXG1 overexpression (Fig. 8F).

FOXG1 inhibits osteoclastic differentiation

Then, we investigated the effect of FOXG1 on osteoclast differentiation. We detected the expression of FOXG1 and osteoclast marker CTSK by immunofluorescence. The results showed that fewer FOXG1 colocalized with CTSK in the femoral bone tissues of OVX mice. After FOXG1

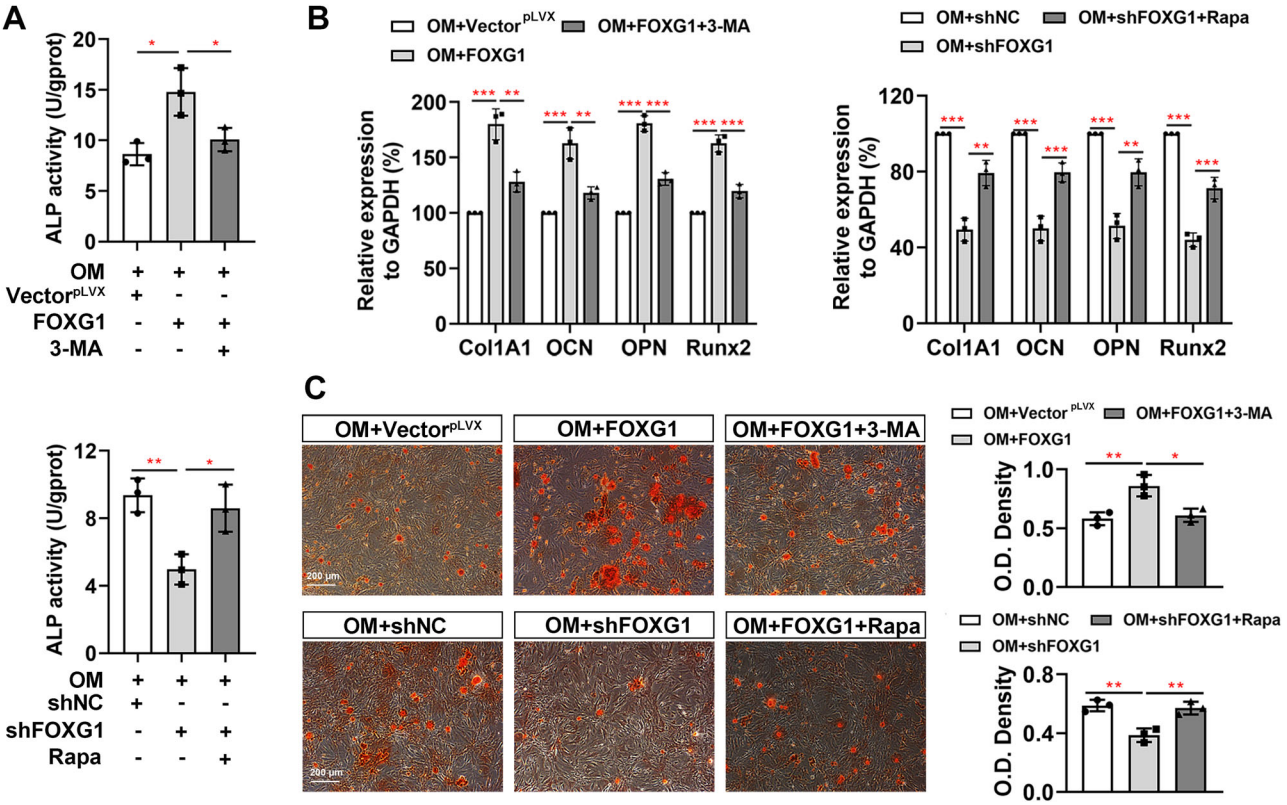

Fig. 3 | FOXG1 induces osteogenic differentiation by regulating autophagy in BMSCs. After lentivirus infection, 100 nM of Rapamycin (autophagy activator) or 5 mM 3-MA (autophagy inhibitor) was added to BMSCs, then, BMSCs were cultured in OM. **A** ALP activity was detected using an ALP activity detection kit. **B** The mRNA expression levels of Col1A1, OCN, OPN, and Runx2 were detected by RT-qPCR. **C** The calcium deposition was determined by Alizarin red staining. Scale bar, 200 μm. Data represented mean ± SD ($n = 3$ biological replicates). $^{*}P < 0.05$; $^{**}P < 0.01$; $^{***}P < 0.001$.

overexpression, more co-localization of FOXG1 and CTSK revealed that AAV-mediated FOXG1 infected osteoclast. (Supplementary Fig. 6). Further, osteoclast activity was measured by osteoclast-specific TRAP staining. The results showed that the number of osteoclasts increased in femur tissue from OVX mice, whereas this trend was alleviated after FOXG1 overexpression (Fig. 9A). The expression levels of osteoclast-related markers were also detected. We found that expression levels of Acp5, Ctsk, and Nfatc1 were upregulated in the femur from OVX mice, but their expression was reduced by FOXG1 overexpression (Fig. 9B). In vitro, RANKL was used to induce osteoclast differentiation of RAW 264.7 cells. TRAP-positive cells with more than three nuclei were considered osteoclasts. TRAP staining exhibited that FOXG1 overexpression in cells blocked osteoclast differentiation (Fig. 9C). The expression levels of Acp5, Ctsk, and Nfatc1 were suppressed by FOXG1 overexpression during osteoclast formation (Fig. 9D). These findings suggested that FOXG1 inhibited osteoclast differentiation. Moreover, we further investigated the mechanism of how FOXG1 suppresses osteoclast differentiation. We found that autophagy increased in RANKL induced-osteoclasts, which was further increased after FOXG1 overexpression (Fig. 9E). Inflammatory responses promote osteoclast differentiation. Results also showed that the expression of IL-6 and TNF-α increased in RANKL-induced osteoclasts, while FOXG1 overexpression inhibited this trend (Fig. 9F), suggesting that FOXG1 may play a role in inhibiting osteoclast differentiation more by inhibiting inflammation.

Discussion

The osteogenic differentiation of BMSCs is crucial for bone formation, and its imbalance results in osteoporosis[19]. We identified a key role of FOXG1 in the control of osteogenesis via BMSCs (Fig. 10). FOXG1 is a nuclear-cytosolic transcription factor and participates in a large number of cell functions, such as cell replication, differentiation, and apoptosis[20]. FOXG1 is highly expressed in skeletal tissues and mouse mesenchymal cells, and silencing FOXG1 inhibits the expression of osteogenic markers[21]. Kimira et al. reported that prolyl-hydroxyproline promotes osteogenic differentiation via regulating FOXG1 expression[8]. Crosstalk between osteogenesis and autophagy is accepted as a novel mechanism of osteoporosis[22]. FOXG1 has been reported to take part in the activation of autophagy, its knockdown reduces the autophagy activity and causes the accumulation of ROS[5]. FOXG1 also promotes autophagy to enhance the radiosensitivity of glioma cells[7]. The above supports our assumption that FOXG1 plays an important role in osteogenesis.

To investigate the role of FOXG1 in osteogenesis, in our study, we overexpressed or silenced FOXG1 in BMSCs from mice. We found that FOXG1 expression was gradually increased during osteoblast differentiation. Both ALP activity and calcium deposition are biomarkers of osteogenic differentiation[23]. FOXG1 promoted ALP activity and calcium deposition. Moreover, the expression levels of osteogenic markers (Col1A1, OCN, OPN, and Runx2) were significantly upregulated by FOXG1 overexpression. These findings suggested that FOXG1 promoted osteogenic differentiation. Furthermore, we established the OVX mouse model and overexpressed FOXG1 in OVX mice. Our in vivo experiments demonstrated that FOXG1 upregulation was observed in OVX mice, and the bone loss induced by OVX was efficaciously rescued after FOXG1 overexpression. Osteoporosis is caused by the collapse of the balance between bone formation and bone resorption. OVX may stimulate a physiological stress response in mice, which leads to the upregulation of FOXG1 expression to try to restore the balance between bone formation and bone resorption. However, this protective effect is not enough to hinder the pathological process. Thus, there is a situation in which FOXG1 upregulation but the inhibition of osteoblast differentiation is not prevented. Then we isolated BMSCs from these groups. FOXG1 overexpression in OVX mice-derived BMSCs increased the ALP activity and calcium deposition. These

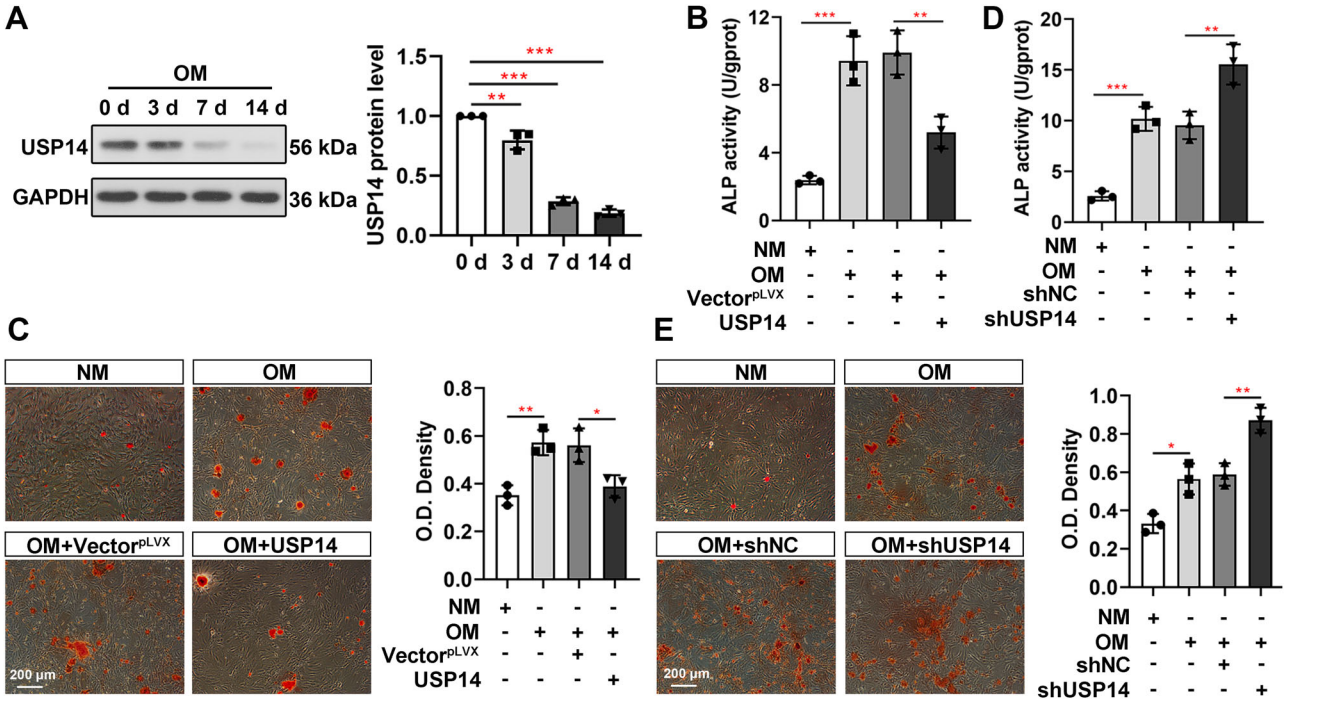

Fig. 4 | USP14 inhibits osteogenic differentiation of mice-derived BMSCs. **A** BMSCs were incubated in osteogenic medium for 0, 3, 7, or 14 days, then, the protein expression level of USP14 was detected by western blot. BMSCs were infected with USP14 overexpression lentivirus (USP14), 48 h after infection, **B** ALP activity was detected using an ALP activity detection kit. **C** The calcium deposition was determined by Alizarin red staining. Scale bar, 200 μm. BMSCs were infected with shUSP14 lentivirus (shUSP14), 48 h after infection, **D** ALP activity was detected using an ALP activity detection kit. **E** The calcium deposition was determined by Alizarin red staining. Scale bar, 200 μm. Data represented mean ± SD ($n = 3$ biological replicates). $^{*}P < 0.05$; $^{**}P < 0.01$; $^{***}P < 0.001$.

findings confirmed that FOXG1 promoted osteoblast differentiation in BMSCs and played a protective role in osteoporosis.

Autophagy is a critical self-degradative process that maintains cellular homeostasis via decomposing and eliminating damaged proteins and organelles[24,25]. It is recognized that autophagy and osteogenesis are closely related. The increase of autophagy has been confirmed to enhance the osteogenic differentiation ability of BMSCs[22,26]. In our study, FOXG1 enhanced autophagy in BMSCs, which was proved by increased the formation of autophagosomes, Beclin 1 expression, and the LC3-II/LC3-I ratio. Our data was consistent with previous research about the effect of FOXG1 on autophagy[27]. Moreover, autophagy activator Rapa rescues the autophagy in BMSCs and attenuates the osteoporotic phenotype in OVX mice, whereas autophagy inhibitors 3-MA and CQ show the opposite effect[28,29]. Here, our findings revealed that 3-MA and CQ reversed the osteogenic differentiation induced by FOXG1 overexpression, but Rapa promoted this effect on FOXG1 knockdown BMSCs, suggesting that FOXG1 induces the osteogenic differentiation via regulating autophagy. Moreover, autophagy is involved in the mediating effect of estrogen on the osteogenic potential of osteoblasts. Estrogen regulates the autophagy of osteoblasts and positively regulates the survival and function of osteoblasts[30]. However, without estrogen, osteoblasts succumb to stress-induced apoptosis, ultimately leading to osteoporosis. It has been reported that silencing FOXG1 reduces estrogen concentration in primary granulosa cells and leads to decreased expression of genes essential for estrogen synthesis, suggesting that FOXG1 promotes estrogen synthesis[31]. Therefore, FOXG1 overexpression may promote autophagy by promoting estrogen synthesis, thereby saving osteoblasts and improving osteoporosis.

Furthermore, FOXG1, as a transcriptional repressor, is involved in many diseases by regulating downstream genes, such as Wnt5a, p21, and AIB2[32–34]. In our study, we predicted that there were FOXG1 binding sites on the USP14 promoter. USP14 inhibition protects murine osteoblastic cells against DEX-induced apoptosis[17]. Moreover, USP14 inactivation influences proliferation by SQSTM1/p62-mediated selective autophagy[35]. Also, USP14 controls autophagy via negatively regulating K63 ubiquitination of Beclin 1[15]. The inhibition of USP14 promotes autophagy, which alleviates DNA damage repair[18]. Here, we found that USP14 expression was reduced when BMSCs were induced to osteogenic differentiation, and FOXG1 negatively regulated the expression of USP14. The dual-luciferase reported and ChIP-qPCR assays demonstrated that FOXG1 transcriptionally inhibited USP14 via binding to the USP14 promoter. Further, USP14 overexpression blocked the autophagy and osteogenic differentiation effects of FOXG1 on BMSCs. Therefore, our results indicated that FOXG1-mediated BMSC improvement in osteoporosis was related to the inhibition of USP14. As a transcriptional factor, other downstream targets of FOXG1 may be involved in osteogenic differentiation, which will be further conducted in our future studies.

We also investigated the effect of FOXG1 on osteoclast differentiation. The results confirmed that FOXG1 inhibited osteoclast differentiation in mice. Previous studies reported that autophagy promotes osteoclast differentiation and bone resorption[36]. In our results, although FOXG1 promoted autophagy, it inhibited osteoclastic differentiation. In addition to autophagy, inflammatory responses also promote osteoclast differentiation[37,38]. FOXG1 has been reported to inhibit inflammatory factors[39], we examined the effect of FOXG1 on inflammation and our results confirmed that FOXG1 suppressed inflammation. Therefore, we speculate that FOXG1 may play a role in inhibiting osteoclast differentiation more by inhibiting inflammation.

In conclusion, our study confirms that FOXG1 induces BMSC osteogenic differentiation and suppresses osteoclast differentiation, which exerts a protective role in osteoporosis. These findings suggest that targeting FOXG1 may be a promising therapeutic approach for osteogenesis treatment.

Methods

Bioinformatic analysis

One set of gene expression data (accession number: GSE35958) containing BMSCs in the normal group and the osteoporosis group were downloaded from the Gene Expression Omnibus (GEO, https://www.ncbi.nlm.nih.gov/geo/) database, then, the expression profiling of FOXG1

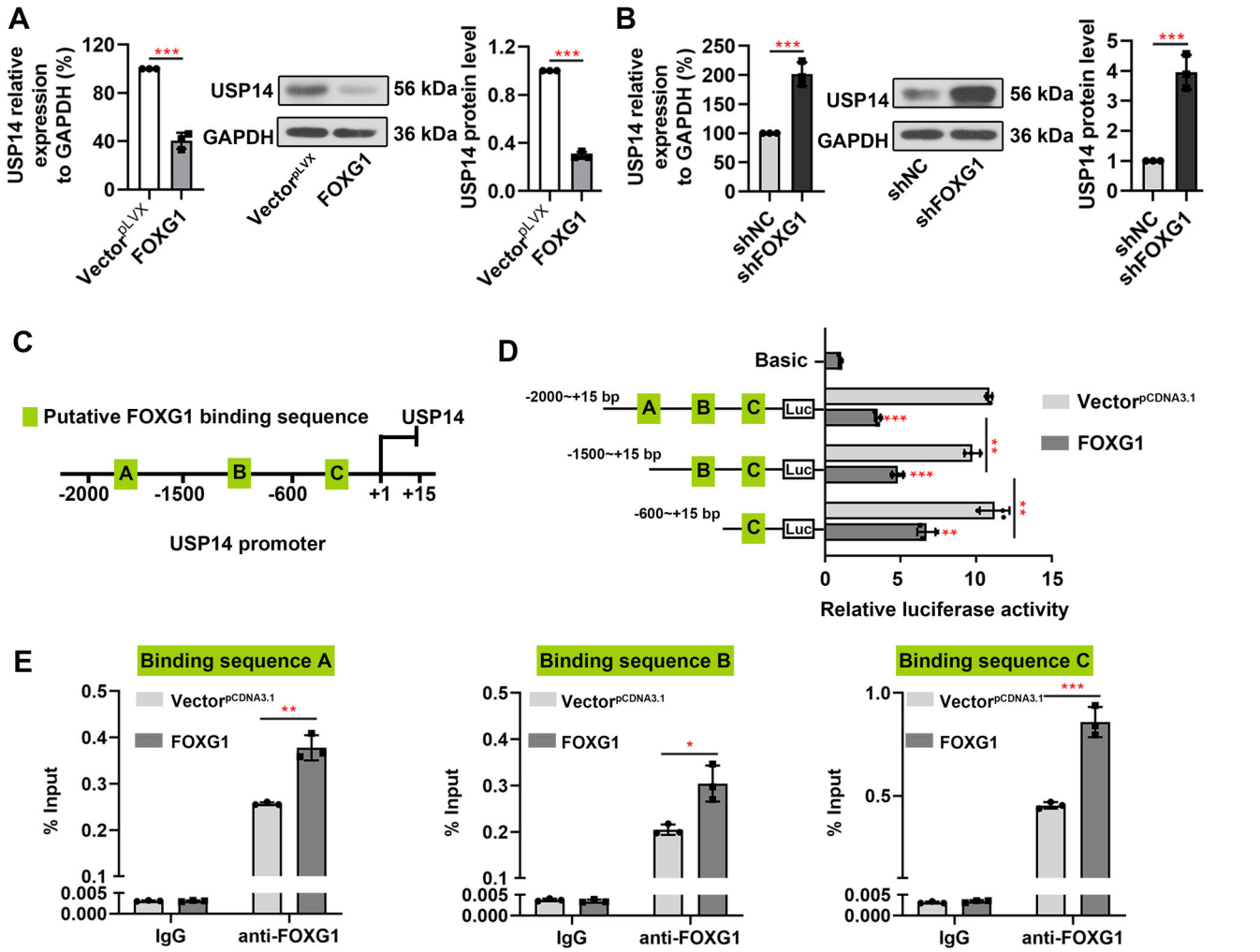

Fig. 5 | FOXG1 inhibits the transcription of USP14. A, **B** BMSCs were infected with FOXG1 overexpression lentivirus (FOXG1) or shFOXG1 lentivirus (FOXG1), 48 h after infection, mRNA and protein expression levels of USP14 were detected by RT-qPCR and western blot. **C** The putative binding sites of FOXG1 on the USP14 promoter. **D** Luciferase reporter plasmids containing the different USP14 promoter fragments were transfected into 293 T cells with FOXG1 overexpression plasmids (FOXG1), 48 h after transfection, the relative luciferase activity was detected by dual-luciferase reported assay. **E** Validation of the FOXG1 binding sites by ChIP–qPCR. ChIP–qPCR data were normalized by the percent input method. Data represented mean ± SD ($n = 3$ biological replicates). $^{*}P < 0.05$; $^{**}P < 0.01$; $^{***}P < 0.001$.

was analyzed by GEO2R. FOXG1 binding sites on the USP14 promoter were predicted using the JASPAR database (http://jaspar.genereg.net/).

Adeno-associated virus (AAV) preparation

For FOXG1 overexpression in vivo, the cDNA of FOXG1 (Accession number: NM_001160112) was inserted into the AgeI/EcoRI site of pAAV-CMV-U6 vector to establish FOXG1 overexpression AAV (AAV-FOXG1). AAV-FOXG1 was further co-transfection into AAV-293 cells (iCell, China) with pHelper vector (Takara, Japan) and pAAV-RC9 vector (Fenghbio, China) for production of viral particles. 72 h after transfection, cells were harvested, lysed by freezing-thawing cycles, and filtered through a 0.45 μm filter.

Experimental design

Eight-week-old female C57BL/6J mice (body weight 20 ± 2 g, specific-pathogen-free grade) were purchased from Jiangsu Huachuang Sino Pharmaceutical Technology Co., Ltd. The animal experiments were approved by the ethics committee of Shengjing Hospital of China Medical University (2021PS161K) and conformed to the ARRIVE guidelines. We have complied with all relevant ethical regulations for animal use. The housing environment conditions are as follows: a room with 21 ± 2 °C temperatures, 55 ± 10% humidity, and a 12:12 light/dark cycle. During experiments, the general healthy status of mice and water consumption were observed and their body weight was recorded every day. Mice were humanely euthanized via CO_2 inhalation if mice quickly lost 15–20% of their body weight. The experiments were not blinded. The sample size of the experimental groups was defined based on previous experience with the models and Source Forge's free online sample size calculator. Mice were randomly assigned to each group using Microsoft Excel. To minimize potential confounders, the mouse surgery order was randomized within each cage.

Establishment of osteoporosis mice

Experiment 1: Twelve mice were randomly divided into Sham and OVX groups ($n = 6$/group). Mice in the OVX group underwent bilateral ovariectomy (OVX), and mice in the Sham group underwent surgery that exposed the ovaries without the excision of ovaries. No mice died in this experiment.

Experiment 2: Fifty-six mice were randomly divided into Sham and OVX groups. There were 12 mice in Sham group and 44 mice in OVX group. OVX model was established as above. Seven mice in OVX group died after surgery and 1 was used for preliminary experiments. One week after surgery, the remained OVX mice were randomly divided into OVX, OVX + AAV-vector, and OVX + AAV-FOXG1 groups ($n = 12$/group). Mice in the OVX + AAV-FOXG1 and OVX + AAV-vector groups were

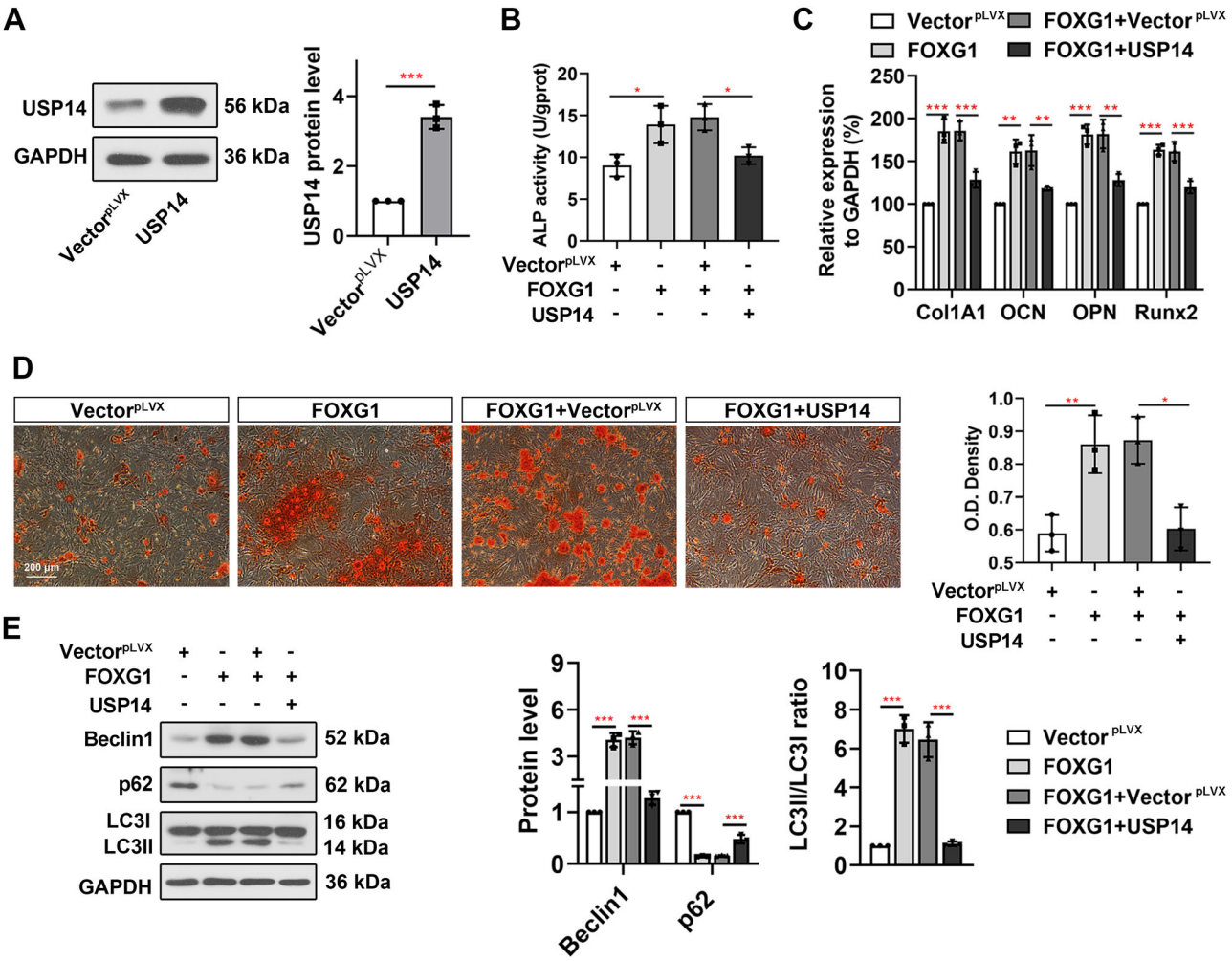

Fig. 6 | FOXG1 promotes autophagy and osteogenic differentiation by regulating USP14 in BMSCs. A BMSCs were infected with USP14 overexpression lentivirus (USP14), 48 h after infection, the protein expression levels of USP14 were detected by western blot. **B** BMSCs were co-infected with USP14 overexpression lentivirus (USP14) and FOXG1 overexpression lentivirus (FOXG1), 48 h after infection, BMSCs were cultured in osteogenic medium, then, ALP activity was detected using an ALP activity detection kit. **C** The mRNA expression levels of Col1A1, OCN, OPN, and Runx2 were detected by RT-qPCR. **D** The calcium deposition was determined by Alizarin red staining. Scale bar, 200 μm. **E** The protein expression levels of Beclin1, p62, and LC3I/II were detected by western blot. Data represented mean ± SD ($n = 3$ biological replicates). $^{*}P < 0.05$; $^{**}P < 0.01$; $^{***}P < 0.001$.

injected with AAV-FOXG1 and empty AAV (AAV-vector) by femoral intramedullary cavity injection, respectively. Six mice in each group were used for micro-CT scanning and pathological examination, and others were used for western blot analysis. Eight weeks after surgery, mice were euthanized via CO_2 inhalation, and femur tissues were collected.

Isolation and identification of BMSCs

Experiment 1: Five C57BL/6J mice were randomly selected as Sham and 13 mice were used for OVX modeling. Two mice died after surgery. The remaining 11 OVX mice were randomly divided into OVX ($n = 5$), OVX + AAV-vector ($n = 3$), and OVX + AAV-FOXG1 ($n = 3$). Eight weeks after surgery, femur tissues were collected from these mice for BMSC isolation.

Experiment 2: Thirteen C57BL/6J mice without OVX or AAV infection were subjected to BMSC isolation.

Bone marrow cells were flushed with a syringe from the femur and tibia of mice, and then were cultured in MEM medium (containing 15% fetal bovine serum) at 37 °C with 5% CO_2. Non-adherent cells were removed via changing the culture medium. For osteogenic differentiation, BMSCs were cultured in osteogenic medium (OM, containing 10^{-2} M β-glycerol phosphate, 50 mg/ml ascorbic acid, and 15% FBS) for 0, 3, 7, or 14 days. When each time point was reached, BMSCs were collected for further experiments.

For flow cytometric analysis on cell surface markers, BMSCs were incubated with CD29 (11-0291-80, Thermo), CD34 (11-0341-81, Thermo), CD45 (FITC-65087, Proteintech), and CD90 (FITC-65088, Proteintech) primary antibodies for 30 min, then, BMSCs were analyzed via flow cytometry (NovoCyte, Agilent, USA). Gating images of flow cytometry are shown in Supplementary Fig. 8.

Osteoclast culture

The RAW264.7 cell line was purchased from iCell (China) and incubated with DMEM medium supplemented with 10% fetal bovine serum at 37 °C. Then, the RAW264.7 cells were cultured with RANKL (50 ng/ml) to induce osteoclast differentiation.

Lentiviral preparation and infection

For overexpression, the coding sequence (CDS) of FOXG1 or USP14 was inserted into pLVX-IRES-puro lentiviral vectors (Fenghbio, China) to produce FOXG1 overexpression lentiviral (FOXG1) or USP14 overexpression lentiviral (USP14). Empty lentiviral vectors (Vector) were regarded as a negative control. For knockdown, shFOXG1 was inserted into pLVX-shRNA1 lentiviral vectors (Fenghbio, China) to construct FOXG1 knockdown lentiviral (shFOXG1), and nontargeting shRNA lentiviral vectors (shNC) were used as a negative control. The shRNA targeting

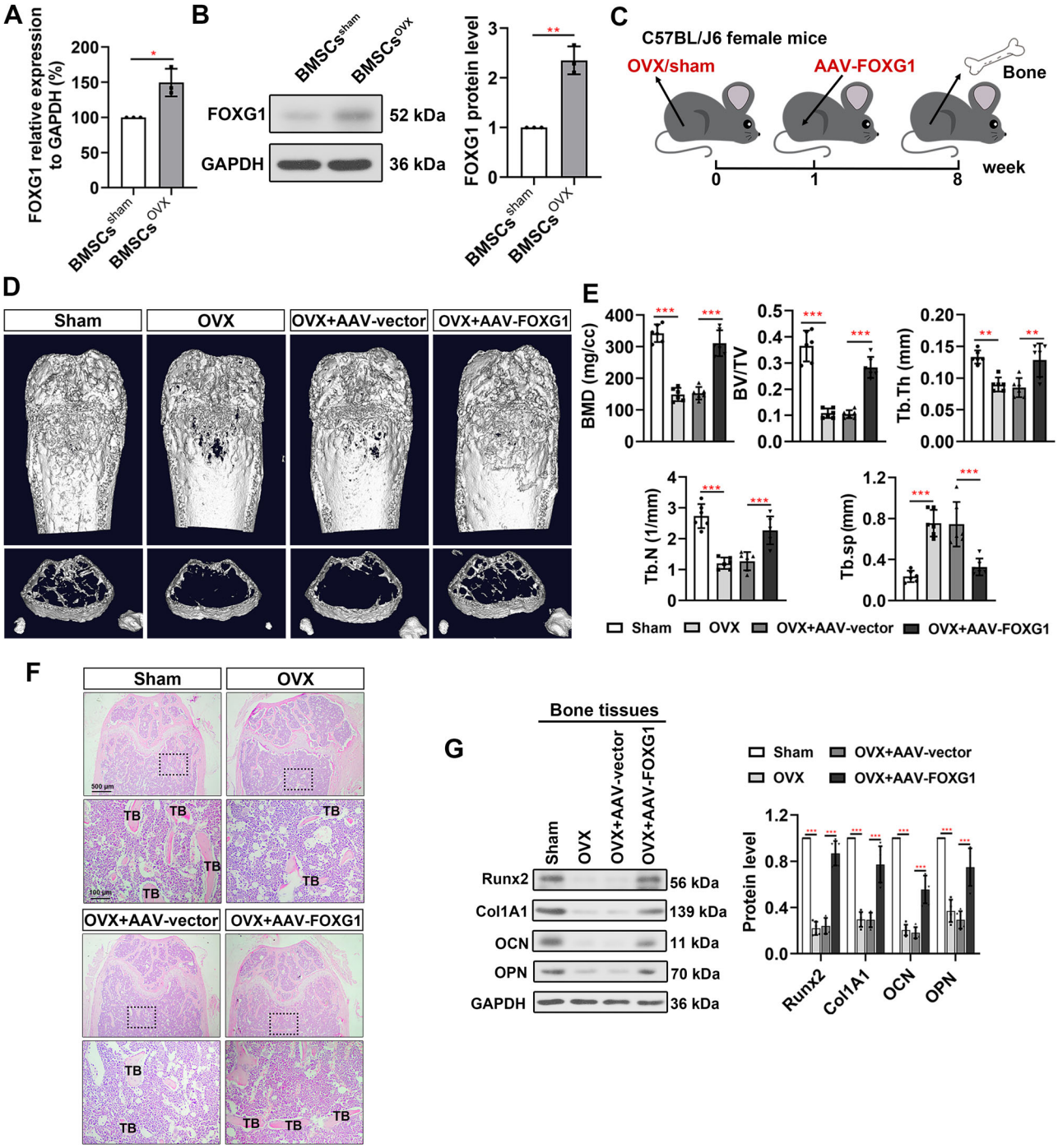

Fig. 7 | FOXG1 alleviates OVX-induced osteoporosis mice. A, **B** BMSCs were isolated from the femurs of mice in the Sham or OVX group, then, the mRNA and protein expression levels of FOXG1 were detected by RT-qPCR and western blot. **C** Schematic diagram showing the OVX mouse modeling experimental procedures. One week after OVX surgery, mice in the OVX + AAV-FOXG1 and OVX + AAV-vector were injected with FOXG1 overexpression AAV (AAV-FOXG1) and empty AAV (AAV-vector) by femoral intramedullary cavity injection, respectively. Eight weeks after surgery, femur tissues were collected for (**D**) micro-CT to quantify (**E**) bone mineral density (BMD), bone volume/total volume (BV/TV), trabecular thickness (Tb. Th), trabecular bone number (Tb. N), and trabecular space (Tb. Sp). **F** Representative images of H&E staining of decalcified bone sections. Scale bar, 500 μm or 100 μm. TB, trabecular bone. **G** The protein expression levels of Col1A1, OCN, OPN, and Runx2 were detected by western blot. Data represented mean ± SD ($n = 3$ biological replicates in cell experiments, $n = 6$ biological replicates in animal experiments). $^{*}P < 0.05$; $^{**}P < 0.01$; $^{***}P < 0.001$.

FOXG1 was 5′-AGTCCTCGTTCAGCATCAACA-3′. The infected cells were selected with G418 to establish stable cell lines.

Histology

The femurs from mice were embedded in paraffin, deparaffinized, and then stained with haematoxylin for 5 min. After treatment with 1% hydrochloric acid alcohol and distilled water, the samples were stained with eosin for 3 min. For Tartrate-resistant acid phosphatase (TRAP) staining, TRAP solution (Solarbio, China) was added to the sections and incubated at 37 °C for 30 min. Then, hematoxylin was used to counterstain the samples for 3 min and returned blue for 5 min. Finally, the samples were sealed with neutral gum and were imaged by a BX53 microscope (OLYMPUS, Japan).

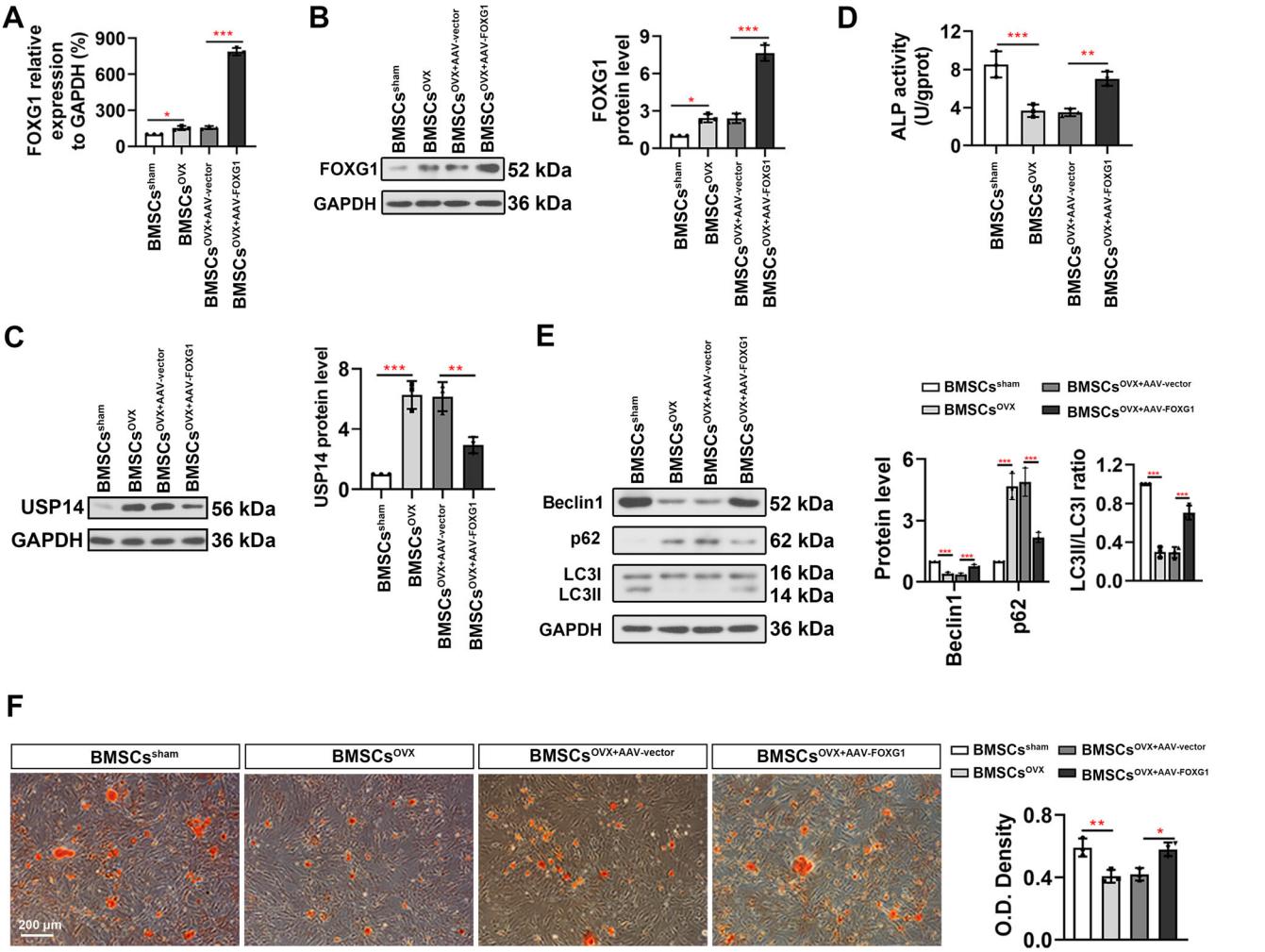

Fig. 8 | FOXG1 promotes osteogenic differentiation of BMSCs from OVX-induced osteoporosis mice. BMSCs were isolated from the femurs of mice, and (**A**, **B**) BMSCs were isolated from the femurs of mice, and the mRNA and protein expression levels of FOXG1 were detected by RT-qPCR and western blot. **C** The protein expression level of USP14 was detected. **D** BMSCs were cultured in osteogenic medium, then, ALP activity was detected using an ALP activity detection kit. **E** The protein expression levels of Beclin1, p62, and LC3I/II were detected by western blot. **F** The calcium deposition was determined by Alizarin red staining. Scale bar, 200 μm. Data represented mean ± SD ($n = 3$ biological replicates). $^{*}P < 0.05$; $^{**}P < 0.01$; $^{***}P < 0.001$.

Transmission electron microscopy (TEM) analysis

BMSCs were harvested and incubated with electron microscopy-grade fixative buffer (Servicebio, China). After washing three times, cells were per-embedded in 1% agar. Then the samples were post-fixed with 1% osmic acid for 2 h and sequentially dehydrated in alcohol (30%, 50%, 70%, 80%, 100%, and 100%) for 20 min, and finally, with 100% acetone twice. Samples were cut into slices after infiltration embedding and polymerization. Subsequently, slices were stained with 2% uranyl acetate saturated alcohol solution for 8 min. After washing three times, slices were stained with 2.6% lead citrate for 8 min. The images were observed by TEM (H-7650, Hitachi, Japan).

Quantitative real-time PCR (RT-qPCR)

Total RNA was extracted from BMSCs by TRIpure (BioTeke, China). cDNA was synthesized using BeyoRT II M-MLV Reverse Transcriptase (Beyotime, China). RT-qPCR for the indicated genes was carried out using ExicyclerTM 96 fluorescence quantifier (Bioneer, Korea). The sequences of the primers were 5′-TACCGACTTGTTCCCTAT-3′ and 5′-TTTCCACCTCTTCTTTGA-3′ for Beclin1, 5′-GCGACAAGAAGAACGGCAAGT-3′ and 5′-ACAGGT TGTGGCGGATGG-3′ for FOXG1, 5′-GTGCCTGAACTCAAAGA-3′ and 5′-CAGAATAATAGGTGGGATA-3′ for USP14, 5′-GCAGCACTCCATAT CTCTACT-3′ and 5′-TTCCGTCAGCGTCAACAC-3′ for Runx2, 5′-CGCC ATCAAGGTCTACTGC-3′ and 5′-GAATCCATCGGTCATGCTCT-3′ for COl1A1, 5′-GAGGGCAATAAGGTAGTGAA-3′ and 5′-CATAGATGCGT TTGTAGGC-3′ for OCN, 5′-CACTCCAATCGTCCCTAC-3′ and 5′-AG ACTCACCGCTCTTCAT-3′ for OPN, and 5′-AACCAAGCCTTCTT CCTCC-3′ and 5′-TGCTGTCCCGAATGTCTCC-3′ for LC3. The gene expression is normalized to the housekeeping gene GAPDH and reflects the relative percentage of expression towards the housekeeping genes.

Western blot

Protein samples were separated by sodium dodecyl sulfate (SDS)-polyacrylamide gels and then transferred to polyvinylidene fluoride (PVDF) membranes (Millipore, USA). After blocking, the membranes were incubated with anti-p62 (AF5384, Affinity, 1:1000 dilution), anti-LC3 (AF5402, Affinity, 1:500 dilution), anti-USP14 (DF9982, Affinity, 1:1000 dilution), anti-Beclin 1 (AF5128, Affinity, 1:1000 dilution), anti-FOXG1 (DF13235, Affinity, 1:1000 dilution), anti-Runx2 (AF5186, Affinity, 1:1000 dilution), anti-Col1A1 (AF7001, Affinity, 1:500 dilution), anti-OCN (DF12303, Affinity, 1:500 dilution), anti-OPN (A1361, Abclonal, 1:1000 dilution) or anti-GAPDH (60004-1-Ig, Proteintech, 1:10000 dilution) overnight at 4 °C. Then, the membranes were incubated with goat anti-rabbit IgG-HRP (SE134, Solarbio, 1:3000 dilution) or goat anti-mouse IgG-HRP (SE131, Solarbio, 1:3000 dilution). After ECL color rendering, the optical density of

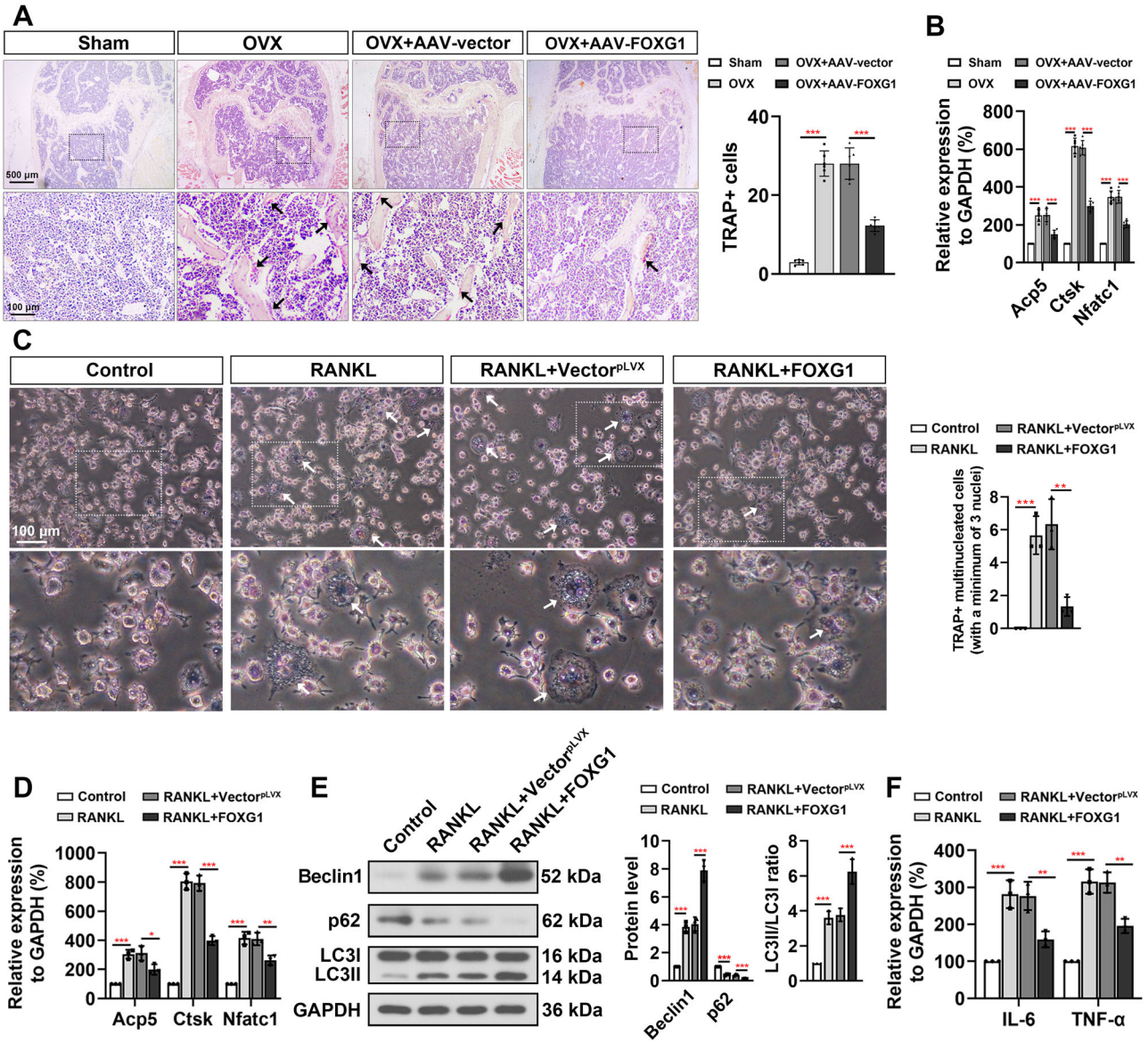

Fig. 9 | FOXG1 inhibits osteoclastic differentiation. **A** Representative images of TRAP staining of femoral tissue sections. Scale bar, 500 μm and 100 μm. The black arrow indicates TRAP+ cells. **B** The mRNA expression of Acp5, Ctsk, and Nfatc1 in femoral tissues. **C** Raw264.7 cells were infected with FOXG1 lentivirus, 48 h after infection, osteoclast differentiation was induced by RANKL for 7 days, and TRAP staining was performed to detect the osteoclast formation. Scale bar, 100 μm. The white arrow indicates TRAP+ cells containing more than three nuclei. **D** The mRNA expression of Acp5, Ctsk, and Nfatc1 was detected. **E** The proteins of Beclin1, LC3I/II, and p62 were detected. **F** The mRNA expression of IL-6 and TNF-α was detected. Data represented mean ± SD ($n = 3$ biological replicates in cell experiments, $n = 6$ biological replicates in animal experiments). $^{*}P < 0.05$; $^{**}P < 0.01$; $^{***}P < 0.001$.

the target band was detected using Gel-Pro-Analyzer software. All original immunoblot images are shown in Supplementary Fig. 7.

Alkaline phosphatase (ALP) analysis

BMSCs were seeded in osteogenic medium for 7 days and were performed to ultrasonic fragmentation. After centrifugation, the resulting supernatant was utilized to measure protein content. The ALP activity was detected by an Alkaline Phosphatase Assay Kit (Jiancheng, China) according to the manufacturer's instructions.

Alizarin red staining

After 14 days of osteogenic induction, Alizarin Red staining was conducted to detect calcium deposition. BMSCs were fixed with 60% isopropanol for 15 min and then washed three times, followed by staining with 1% Alizarin red for 10 min. The images were observed with a BX53 microscope (OLYMPUS, Japan).

Immunofluorescence (IF)

Cells were grown on glass coverslides and fixed with 4% paraformaldehyde for 15 min. After washing with PBS three times, cells were incubated with 0.1% tritonX-100 for 30 min, followed by incubation with anti-LC3 (sc-376404, Santa, 1:50 dilution), FOXG1 (AP9793C, Abcepta, 1:100 dilution), CTSK (Sc-48353, Santa, 1:50 dilution) overnight at 4 °C. Then, cells were incubated with Cy3-labeled goat anti-mouse IgG (A-21424, Invitrogen, 1:200 dilution), Cy3-labeled goat anti-rabbit IgG (ab6939, Abcam, 1:200 dilution) or FITC-labeled goat anti-mouse IgG (ab6785, Abcam, 1:200 dilution) for 60 min. DAPI solution was then used to counterstain the nucleus. Finally, cells were imaged by a BX53 microscope (OLYMPUS, Japan).

Dual-luciferase reported assay

HEK 293T cells were seeded to 12-well plates and co-transfected with FOXG1 overexpression plasmids and luciferase reporter plasmids

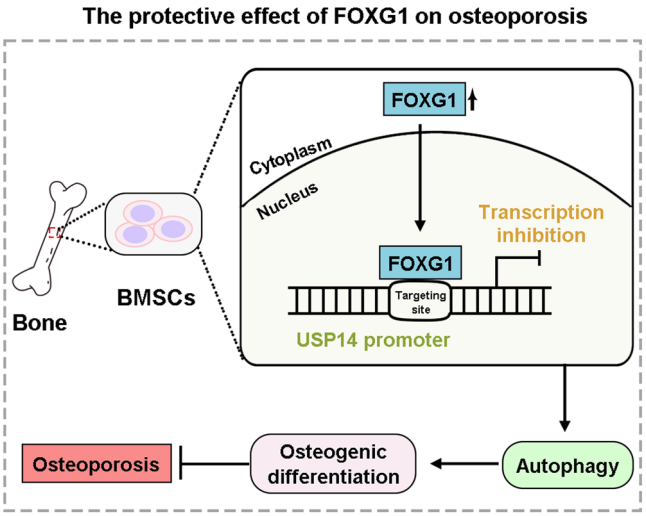

Fig. 10 | Schematic diagram depicting the effect of FOXG1 on osteoporosis. FOXG1 inhibits USP14 transcription via promoter binding to promote autophagy in BMSCs, thereby alleviating osteoporosis progression.

containing the different USP14 promoter fragments. 48 h post-transfection, cells were lysed with lysis buffer and the luciferase activity was detected by Dual Luciferase Assay Kit (KeyGEN, China).

Chromatin immunoprecipitation (ChIP)-qPCR

ChIP assays were performed via a ChIP Assay Kit (Beyotime, China). Briefly, cells were collected and crosslinked for 10 min with 1% formaldehyde. After washing with PBS, cells resuspended with SDS Lysis Buffer and then were sonicated to generate DNA fragments. Next, the samples were diluted with ChIP Dilution Buffer overnight at 4 °C. 20 μl of samples without primary antibodies were used as input controls. The remaining samples were incubated with anti-FOXG1 or rabbit IgG with Protein A + G Agarose/Salmon Sperm DNA. Immunoprecipitated complexes and input controls were eluted with Elution buffer and DNA was purified for RT-qPCR detection of target genes.

Statistics and reproducibility

Three biological replicates were performed in cell experiments, and six biological replicates were performed in animal experiments. For data measurements, individual mice were used as experiment units. All the results were analyzed with GraphPad Prism Version 9.0 and were displayed as mean ± standard (SD). All data presented a normal distribution according to the Shapiro–Wilk test. Comparisons were assessed via Student's *t*-test or one-way ANOVA analysis. Error bars indicate SD. $P < 0.05$ (95% confidence interval) was considered as statistical significance.

Reporting summary

Further information on research design is available in the Nature Portfolio Reporting Summary linked to this article.

Data availability

The source data behind the graphs can be found in Supplementary Data and unprocessed Western blots in Supplementary Fig. 7. All other data of this study are available on request to the corresponding author.

Received: 18 February 2024; Accepted: 19 December 2024;
Published online: 15 January 2025

References

1. Tu, K. N. et al. Osteoporosis: a review of treatment options. *P T* **43**, 92–104 (2018).
2. Sinha, P. et al. Loss of Gsα early in the osteoblast lineage favors adipogenic differentiation of mesenchymal progenitors and committed osteoblast precursors. *J. Bone Min. Res.* **29**, 2414–2426 (2014).
3. Saidak, Z., Haÿ, E., Marty, C., Barbara, A. & Marie, P. J. Strontium ranelate rebalances bone marrow adipogenesis and osteoblastogenesis in senescent osteopenic mice through NFATc/Maf and Wnt signaling. *Aging Cell* **11**, 467–474 (2012).
4. Roth, M. et al. FoxG1 and TLE2 act cooperatively to regulate ventral telencephalon formation. *Development* **137**, 1553–1562 (2010).
5. He, Z. H. et al. FOXG1 promotes aging inner ear hair cell survival through activation of the autophagy pathway. *Autophagy* **17**, 4341–4362 (2021).
6. Hettige, N. C. & Ernst, C. FOXG1 dose in brain development. *Front. Pediatr.* **7**, 482 (2019).
7. Xiao, N. et al. FOXG1 mediates the radiosensitivity of glioma cells through regulation of autophagy. *Int. J. Radiat. Biol.* **97**, 139–148 (2021).
8. Kimira, Y. et al. Collagen-derived dipeptide prolyl-hydroxyproline promotes osteogenic differentiation through Foxg1. *Cell Mol. Biol. Lett.* **22**, 27 (2017).
9. Benisch, P. et al. The transcriptional profile of mesenchymal stem cell populations in primary osteoporosis is distinct and shows overexpression of osteogenic inhibitors. *PLoS ONE* **7**, e45142 (2012).
10. Yoshida, G. et al. Degradation of the NOTCH intracellular domain by elevated autophagy in osteoblasts promotes osteoblast differentiation and alleviates osteoporosis. *Autophagy* **18**, 2323–2332 (2022).
11. He, Z. H. et al. The nuclear transcription factor FoxG1 affects the sensitivity of mimetic aging hair cells to inflammation by regulating autophagy pathways. *Redox Biol.* **28**, 101364 (2020).
12. Borodovsky, A. et al. A novel active site-directed probe specific for deubiquitylating enzymes reveals proteasome association of USP14. *Embo J.* **20**, 5187–5196 (2001).
13. Lee, B. H. et al. Enhancement of proteasome activity by a small-molecule inhibitor of USP14. *Nature* **467**, 179–184 (2010).
14. Srinivasan, V. et al. Dynamic interaction of USP14 with the chaperone HSC70 mediates crosstalk between the proteasome, ER signaling, and autophagy. *iScience* **23**, 100790 (2020).
15. Xu, D. et al. USP14 regulates autophagy by suppressing K63 ubiquitination of Beclin 1. *Genes Dev.* **30**, 1718–1730 (2016).
16. Moghadami, A. A. et al. Inhibition of USP14 induces ER stress-mediated autophagy without apoptosis in lung cancer cell line A549. *Cell Stress Chaperones* **25**, 909–917 (2020).
17. Zhou, P. et al. Matrine derivate MASM protects murine MC3T3-E1 osteoblastic cells against dexamethasone-induced apoptosis via the regulation of USP14/p53. *Artif. Cells Nanomed. Biotechnol.* **47**, 3720–3728 (2019).
18. Sharma, A. et al. USP14 regulates DNA damage repair by targeting RNF168-dependent ubiquitination. *Autophagy* **14**, 1976–1990 (2018).
19. Deans, R. J. & Moseley, A. B. Mesenchymal stem cells: biology and potential clinical uses. *Exp. Hematol.* **28**, 875–884 (2000).
20. Pancrazi, L. et al. Foxg1 localizes to mitochondria and coordinates cell differentiation and bioenergetics. *Proc. Natl. Acad. Sci. USA* **112**, 13910–13915 (2015).
21. Teixeira, C. C. et al. Foxo1, a novel regulator of osteoblast differentiation and skeletogenesis. *J. Biol. Chem.* **285**, 31055–31065 (2010).
22. He, M. et al. METTL14 regulates osteogenesis of bone marrow mesenchymal stem cells via inducing autophagy through m6A/IGF2BPs/Beclin-1 signal axis. *Stem Cells Transl. Med* **11**, 987–1001 (2022).
23. Grottkau, B. E., Hui, Z., Yao, Y. & Pang, Y. Rapid fabrication of anatomically-shaped bone scaffolds using indirect 3D printing and perfusion techniques. *Int. J. Mol. Sci*. **21** https://doi.org/10.3390/ijms21010315 (2020).

24. Pierrefite-Carle, V., Santucci-Darmanin, S., Breuil, V., Camuzard, O. & Carle, G. F. Autophagy in bone: self-eating to stay in balance. *Ageing Res. Rev.* **24**, 206–217 (2015).
25. Parzych, K. R. & Klionsky, D. J. An overview of autophagy: morphology, mechanism, and regulation. *Antioxid. Redox Signal* **20**, 460–473 (2014).
26. Ceccariglia, S., Cargnoni, A., Silini, A. R. & Parolini, O. Autophagy: a potential key contributor to the therapeutic action of mesenchymal stem cells. *Autophagy* **16**, 28–37 (2020).
27. Mu, Y. R. et al. Role and mechanism of FOXG1-related epigenetic modifications in cisplatin-induced hair cell damage. *Front. Mol. Neurosci.* **16**, 1064579 (2023).
28. Qi, M. et al. Autophagy maintains the function of bone marrow mesenchymal stem cells to prevent estrogen deficiency-induced osteoporosis. *Theranostics* **7**, 4498–4516 (2017).
29. Wan, Y., Zhuo, N., Li, Y., Zhao, W. & Jiang, D. Autophagy promotes osteogenic differentiation of human bone marrow mesenchymal stem cell derived from osteoporotic vertebrae. *Biochem. Biophys. Res. Commun.* **488**, 46–52 (2017).
30. Gavali, S. et al. Estrogen enhances human osteoblast survival and function via promotion of autophagy. *Biochim. Biophys. Acta Mol. Cell Res.* **1866**, 1498–1507 (2019).
31. Yan, X., Hou, L. & Zhang, C. FOXG1 is involved in mouse ovarian functions and embryogenesis. *J. Steroid Biochem. Mol. Biol.* **233**, 106372 (2023).
32. Ni, Y. et al. FOXG1 directly suppresses Wnt5a during the development of the hippocampus. *Neurosci. Bull.* **37**, 298–310 (2021).
33. Chan, D. W. et al. Overexpression of FOXG1 contributes to TGF-beta resistance through inhibition of p21WAF1/CIP1 expression in ovarian cancer. *Br. J. Cancer* **101**, 1433–1443 (2009).
34. Li, J. V. et al. Transcriptional repression of AIB1 by FoxG1 leads to apoptosis in breast cancer cells. *Mol. Endocrinol.* **27**, 1113–1127 (2013).
35. Ming, S. L. et al. Inhibition of USP14 influences alphaherpesvirus proliferation by degrading viral VP16 protein via ER stress-triggered selective autophagy. *Autophagy* **18**, 1801–1821 (2022).
36. Yang, C. et al. TET2 regulates osteoclastogenesis by modulating autophagy in OVX-induced bone loss. *Autophagy* **18**, 2817–2829 (2022).
37. Michalski, M. N. et al. Inflammatory bone loss associated with MFG-E8 deficiency is rescued by teriparatide. *FASEB J.* **32**, 3730–3741 (2018).
38. Tang, W. et al. The growth factor progranulin binds to TNF receptors and is therapeutic against inflammatory arthritis in mice. *Science* **332**, 478–484 (2011).
39. Yun, Q., Ma, S. F., Zhang, W. N., Gu, M. & Wang, J. FoxG1 as a potential therapeutic target for alzheimer's disease: modulating NLRP3 inflammasome via AMPK/mTOR autophagy pathway. *Cell Mol. Neurobiol.* **44**, 35 (2024).

Acknowledgements

This research was funded by the Young Scientists Fund of the National Natural Science Foundation of China (No. 82100939) and the 345 Talent Project of Shengjing Hospital of China Medical University.

Author contributions

Y.Z.: conceptualization and investigation, methodology, formal analysis, writing-original draft. L.Z.: methodology, formal analysis, and visualization. Q.F.: data curation and project administration. Z.L.: conceptualization, supervision, and writing-review and editing.

Competing interests

The authors report no competing interest.

Additional information

Supplementary information The online version contains supplementary material available at https://doi.org/10.1038/s42003-024-07429-2.

Correspondence and requests for materials should be addressed to Ziyun Liu.

Peer review information *Communications Biology* thanks the anonymous reviewers for their contribution to the peer review of this work. Primary Handling Editor: Christina Karlsson Rosenthal. A peer review file is available.

Reprints and permissions information is available at http://www.nature.com/reprints

Publisher's note Springer Nature remains neutral with regard to jurisdictional claims in published maps and institutional affiliations.

Open Access This article is licensed under a Creative Commons Attribution-NonCommercial-NoDerivatives 4.0 International License, which permits any non-commercial use, sharing, distribution and reproduction in any medium or format, as long as you give appropriate credit to the original author(s) and the source, provide a link to the Creative Commons licence, and indicate if you modified the licensed material. You do not have permission under this licence to share adapted material derived from this article or parts of it. The images or other third party material in this article are included in the article's Creative Commons licence, unless indicated otherwise in a credit line to the material. If material is not included in the article's Creative Commons licence and your intended use is not permitted by statutory regulation or exceeds the permitted use, you will need to obtain permission directly from the copyright holder. To view a copy of this licence, visit http://creativecommons.org/licenses/by-nc-nd/4.0/.

© The Author(s) 2025